Coastal Engineering 119 (2017) 1–14

Contents lists available at ScienceDirect

Coastal Engineering

journal homepage: www.elsevier.com/locate/coastaleng

The initial morphological response of the Sand Engine: A process-based modelling study

Arjen P. Luijendijk[a,b,*], Roshanka Ranasinghe[b,c,d], Matthieu A. de Schipper[a,e], Bas A. Huisman[a,b], Cilia M. Swinkels[b], Dirk J.R. Walstra[a,f], Marcel J.F. Stive[a]

[a] Faculty of Civil Engineering and Geosciences, Department of Hydraulic Engineering, Delft University of Technology, Delft, The Netherlands
[b] Deltares, Unit Hydraulic Engineering, Delft, The Netherlands
[c] UNESCO-IHE Institute for Water Education, Department of Water Science and Engineering, Delft, The Netherlands
[d] Water Engineering and Management, Faculty of Engineering Technology, University of Twente, PO Box 217, 7500 AE Enschede, The Netherlands
[e] Shore Monitoring and Research, The Hague, The Netherlands
[f] Deltares, Unit Marine and Coastal Systems, Delft, The Netherlands

ARTICLE INFO

Keywords:
Coastal morphodynamics
Mega nourishment
Sediment transport
Process-based modelling
Delft3D

ABSTRACT

Sand nourishments are presently widely applied to maintain or enhance coastal safety and beach width. Over the last decades, global sand nourishment volumes have increased greatly, and the demand for nourishments is anticipated to increase further in coming decades due to sea level rise. With the increase in nourishment size and the request for more complex nourishment shapes, an adequate prediction of the morphodynamic evolution is of major importance. Yet, neither the skill of current state-of-the-art models for such predictions nor the primary drivers that control the evolution are known. This article presents the results of a detailed numerical modelling study undertaken to examine the model skill and the processes governing the initial morphological response of the Sand Engine and the adjacent coastline. The process-based model Delft3D is used to hindcast the first year after completion of the mega-nourishment. The model reproduces measured water levels, velocities and nearshore waves well. The prediction of the morphological evolution is consistent with the measured evolution during the study period, with Brier Skill Scores in the 'Excellent' range. The model results clearly indicate that the sand eroded from the main peninsular section of the Sand Engine is deposited along adjacent north and south coastlines, accreting up to 6 km of coastline within just one year. Analysis of model results further show that the erosional behaviour of the Sand Engine is linearly dependent on the cumulative wave energy of individual high energy wave events, with the duration of a storm event being more dominant than the maximum wave height occurring during the storm. The integrated erosion volume due to the 12 events with the highest cumulative wave energy density accounts for about 60% of the total eroded volume of the peninsula, indicating that the less energetic wave events, with a higher probability of occurrence, are also important for the initial response of the Sand Engine. A structured model experiment using the verified Delft3D model indicates that wave forcing dominates the initial morphological response of the Sand Engine, accounting for approximately 75% of the total erosion volume in the first year. The vertical tide is the second most important factor accounting for nearly 17% of the total erosion volume, with surge, wind and horizontal tide playing only a minor role.

1. Introduction

Around 75% of the Dutch coast consists of dune areas that provide protection from flooding for the low-lying hinterland [4,30]. Besides that, the sandy coast is also important for ecological and recreational functions and fresh water extraction. Large sections of the Dutch coast have been eroding for centuries [40,36,37,41] which has traditionally been negated with measures such as groynes and/or managed retreat, and since the 1990s, beach/shoreface nourishments. Over the years, the total annual sand nourishment volume along the Dutch coast has steadily increased [10,6] to its present value of approximately 12 million m^3/yr.

In 2008, a Dutch State Committee (the 2nd Delta Committee [33]) provided critical advice for protecting the Dutch coast and the low-

* Corresponding author at: Faculty of Civil Engineering and Geosciences, Department of Hydraulic Engineering, Delft University of Technology, Delft, The Netherlands.
E-mail addresses: arjen.luijendijk@deltares.nl (A.P. Luijendijk), r.ranasinghe@unesco-ihe.org (R. Ranasinghe), m.a.deschipper@tudelft.nl (M.A. de Schipper), bas.huisman@deltares.nl (B.A. Huisman), cilia.swinkels@deltares.nl (C.M. Swinkels), dirkjan.walstra@deltares.nl (D.J.R. Walstra), m.j.f.stive@tudelft.nl (M.J.F. Stive).

http://dx.doi.org/10.1016/j.coastaleng.2016.09.005
Received 17 August 2015; Received in revised form 21 July 2016; Accepted 19 September 2016

Fig. 1. (a) Overview of the Dutch Coast, (b) the Delfland coast showing the location of the Sand Engine (harbour structures in yellow), and (c) aerial photograph of the Sand Engine in July 2011 just after construction (courtesy: Rijkswaterstaat/Joop van Houdt). (For interpretation of the references to colour in this figure caption, the reader is referred to the web version of this paper.)

lying hinterland from the consequences of foreshadowed climate change in the 21st century. In line with a key recommendation of the Delta Committee, an innovative pilot project was developed to achieve a more efficient and sustainable nourishment approach; the Sand Engine ('Zandmotor' in Dutch; hereafter referred to as ZM). This mega-nourishment, built in 2011 along the Delfland coast (see Fig. 1a) consists of a total sediment volume of 21 million m^3. The ZM is a combined beach/shoreface nourishment and consists of a manmade peninsula of about 128 ha [32]. It is expected that over the next 20 years, natural coastal processes will redistribute the sand in the peninsula along the coast between Hoek van Holland and Scheveningen (see Fig. 1b and c), leading to an increase of the footprint of the dunes of 33 ha [20].

The scale of the ZM is unprecedented for a sand nourishment. A comprehensive multidisciplinary five-year monitoring programme was launched in 2011 to monitor and investigate multiple aspects of the initial ZM evolution and coastal response to the ZM. The monitoring campaign provides valuable data on both the forcing conditions and the behaviour of the ZM. However, the observed morphological behaviour cannot be directly related to specific forcing conditions due to the relatively low temporal resolution (~monthly) of the bathymetric surveys of the ZM. A numerical model that to a high degree of detail can reproduce the observed behaviour is therefore the only means of understanding the physical processes that govern the initial evolution of the ZM and the adjacent coast. Therefore, this study uses data acquired in the first 12 months following the completion of the ZM (August 2011–August 2012) in conjunction with state-of-the-art process based morphodynamic modelling to gain insights into the initial response of the nourishment and the adjacent coastline as well as the dominant physical processes. The study period of the first 12 months is selected here to focus on the initial development from a man-made shape to a more smooth shape, a transition which is poorly produced in one line models and vital to the overall development [11]. These insights are anticipated to provide a guide for other large-scale sandy strategies such as artificial islands, land reclamations, (mega-) nourishments worldwide.

Specifically, this study attempts to answer the following:

(1) Can a state-of-the-art 2DH process-based morphodynamic model reproduce the initial morphological evolution of the ZM and the adjacent coast with sufficient accuracy?
(2) What are the forcing conditions that govern the initial morphological evolution of the ZM?

This article is arranged as follows. Section 2 introduces the ZM project and the available monitoring data used in this study. In Section 3 the morphodynamic modelling approach, verification, and the evaluation of the model performance are described. Section 4 investigates the relationships between environmental forcing and the initial morphological evolution of the ZM and the adjacent coast as well as the relative contribution of the different forcing mechanisms. Finally, Section 5 presents the conclusions of this work.

2. The Sand Engine project

2.1. Coastal setting

The Delfland coast is the southern section (16.5 km) of the Holland coast between Hoek van Holland and Scheveningen (see Fig. 1a and b). The nearshore zone is characterised by a rather uniform, gradually sloping beach profile with occasionally a nearshore bar [42]. The width of the dune area from the dune foot varies from narrow (i.e. 150–250 m width) in the central section of the Delfland coast to very wide (500 m width) at Hoek van Holland and just north of the ZM. The dune height is generally between NAP +10 m to NAP +15 m, but locally, dunes can reach over NAP +20 m.

The tide at Scheveningen is semi-diurnal with a spring/neap tidal amplitude of 1.98/1.48 m. The tide is asymmetric with on average a rising period of 4 hours and 21 minutes, while the falling period lasts for about 8 hours. This causes asymmetric alongshore velocities with maximum flood tidal currents of 0.7 m/s (northeast directed) and maximum ebb tidal currents of 0.5 m/s (southwest directed). The 1-year return period surge level at Hoek van Holland is 2.35 m.

The wave climate along the Dutch coast shows little spatial variation but is characterized by a distinct seasonal signal with average winter (Nov–Jan)/summer (Apr–Aug) offshore wave heights (H_s) of 1.7/1 m. Small waves ($H_s < 1$ m) originate predominantly from the northwest, average waves ($1.5\ m < H_s < 3.5$ m) predominantly from both the southwest and northwest while the highest waves ($H_s >$ 4.5 m) originate predominantly from the west and northwest (see Fig. 2a). The 1-year return period offshore wave height H_s is 4 m.

The Delfland coast consists of sandy beaches with an average median grain size (D_{50}) of 242 μm with a standard deviation of about 50 μm [43]. Previous studies on the sediment transport along the Dutch coast indicate a northward longshore transport between 50,000 to 170,000 m^3/year at the location of the ZM [36,35]. Near Hoek van Holland the alongshore sediment transport is completely blocked due to the presence of a large groyne called the *Noorderdam* protruding 4.2 km into sea (see Fig. 1b). In contrast, the relatively small harbour moles of Scheveningen harbour allow sediment bypassing. The Delfland coast is subject to chronic erosion due to the sediment demand by neighbouring tidal inlet systems, relative sea level rise

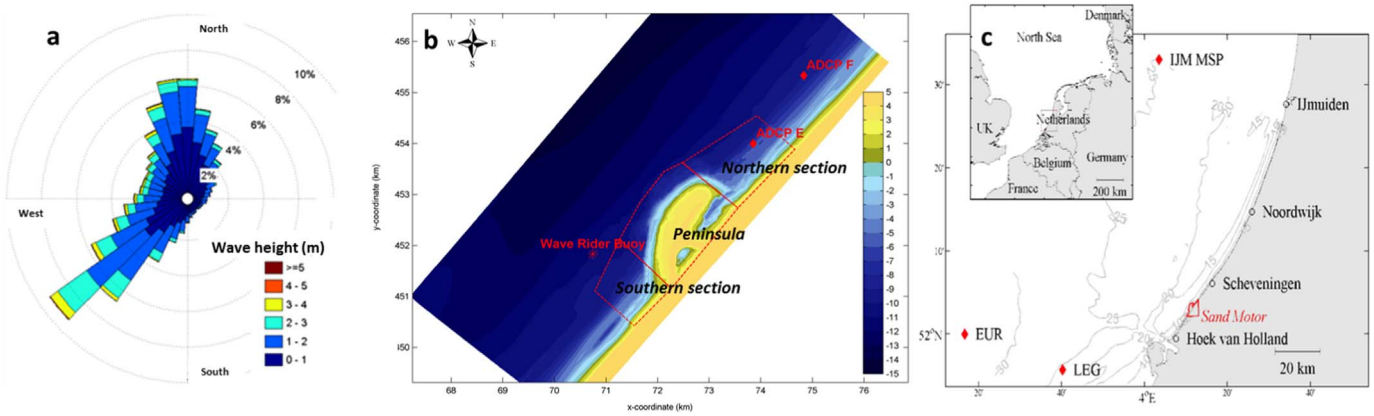

Fig. 2. (a) Wave rose for Europlatform based on 25 years of wave records, (b) the observed ZM bed elevation (in meters) of August 2011 and the locations of two ADCPs, a wave rider buoy, and the three control sections and (c) locations of ZM and relevant measuring stations in the Netherlands (IJM MSP=IJmuiden MunitieStortplaats, EUR=Europlatform, LEG=Licht Eiland Goeree).

and reduced sediment supply from the rivers [36,32]. A dominant factor in the long-term erosional process at the Delfland coast is the presence of the nearby Rhine-Meuse estuary, which acts as a sink for the marine sediments as the fluvial sediment supply has diminished substantially over the last centuries. Based on reconstructions of the coastline using old charts (since 1600 s), Van Rijn [36] estimated that the coastline at the location of the ZM has retreated about 1 km between 1600 and 1990; roughly 2.5 m per year.

After a successful test with three groynes in 1791, twelve additional rock groynes were built in the years thereafter, which locally reduced coastline recession to 0.5–1 m/year [36]. In the period 1807 to 1827 the groyne field was extended northwards with nine more groynes. Thereafter, another 47 groynes were placed until 1930, resulting in a total of 68 groynes along the Delfland coast [13]. Despite these efforts, this coastal stretch remains erosive to date.

A sea change in the Dutch thinking related to coastal protection led to the introduction of sand nourishments from the 1970s along this part of the coast. Since then, the frequency of nourishments has increased to once every 3–4 years. In total, approximately 55 million m^3 of sand has been nourished at the Delfland coast for erosion mitigation and land reclamation (e.g. nature-compensation for the extension of the Port of Rotterdam, Maasvlakte II). In the decade prior to construction of the ZM, nourishment volumes in this stretch had increased to 1.7 million m^3 per year, which is about 100 m^3 of nourished sand per alongshore meter of coast [5].

2.2. The Sand Engine design

The ZM project consists of a large peninsula (see Fig. 2b) with two flanking shoreface nourishments. The main peninsula part is hook shaped with the outer tip curved towards the north. This design and location best fulfilled the multidisciplinary and multi-stakeholders requirements of safety in combination with recreation, nature development and scientific innovation [32]. The most seaward position of the ZM coastline (NAP 0 m contour) protrudes ~1000 m from the original coastline. The cross-shore slope of the peninsula is 1:50, such that the toe of the nourishment is positioned at NAP -8 m and 1500 m from the original coastline. The alongshore base length of the ZM peninsula was ~2000 m just after construction. The northern tip of the peninsula creates a sheltered area that is anticipated to form a nurturing area for different biotic species. Furthermore, the ZM contains a small (~8 ha) lake at the base of the peninsula (see Fig. 1c). This lake is intended to prevent the freshwater lens in the dunes from migrating seaward, which could endanger groundwater extraction from the more landward existing dune area [5]. Sediment for the nourishment was required to be similar to the surrounding coast and regular grain size analysis during construction (after each 0.5 million m^3 of nourished sediment) showed an average D_{50} of 278 μm [15]. The total cost for construction of the peninsula was about € 50 million.

2.3. Data and observations

The post-construction monitoring program included regular bathymetrical, topographical, current, and wave measurements. Table 1 provides an overview of the type of measurements that were undertaken as well as the instruments, frequency and the area that was covered as relevant for this study.

A detailed analysis of the morphological evolution of the ZM in the first 12 months (see Fig. 3) undertaken by [5] has revealed the following main behavioural characteristics.

The most seaward point (at the water line) of the ZM retreated from 960 m to 820 m, indicating a large initial erosion of the tip of the peninsula (see ① in Fig. 3b). The cross-shore profile on the seaward side of ZM became gentler and more similar to the natural slope of the coast. Simultaneously the alongshore extent of the nourishment

Table 1
Overview of monitoring at the Sand Engine during the first 12 months (as relevant for this study).

Measured parameter	Means	Frequency	Coverage (locations in Figure 2b and c)
In-situ bathymetry and topography	Jetski and quad bike	Monthly for the first year; Every two months thereafter	The ZM and adjacent coastal areas (longshore stretch of ~4.7 km)
Wave data	Wave Rider buoy	Continuous from December 2011	Located at 10 m water depth just south of the ZM
	Two platforms	Continuous (part of standard monitoring)	Europlatform 3 (EUR; water depth h=30 m) and Ijmuiden Munitiestortplaats (IJM MSP; h=24 m)
Hydrodynamic data	Two ADCP's	Continuous from April 2012	Located at h=6 and 8 m north of ZM
	Tide gauge	Continuous	Located in Scheveningen Harbour
Sediment samples	Grab samples	Annual	Several cross-shore transects at the ZM
Wind data	Weather station	Continuous	Lichteiland Goeree (LEG) and Hoek van Holland

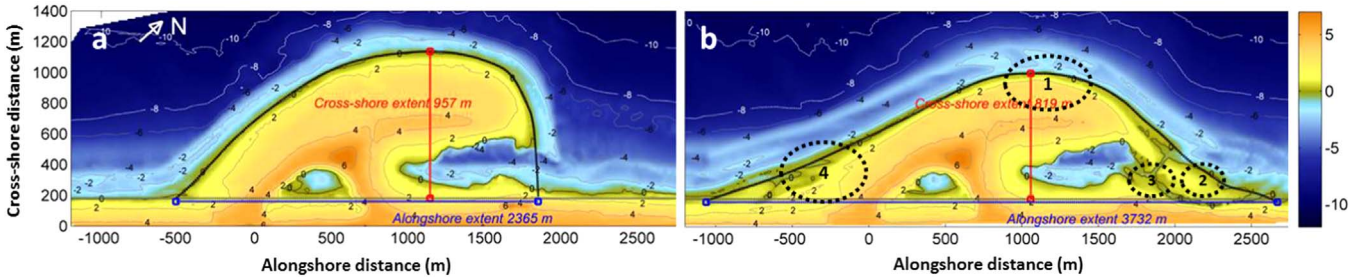

Fig. 3. Observed bed elevations (in meters) in August 2011 (a) and August 2012 (b) after de Schipper et al. [5].

increased from 2370 to 3730 m. Considerable accretion was observed on the adjacent coast to the northeast and southwest of the ZM; the nourishment disperses approximately symmetrically from the centre of the peninsula. On the northern side of the peninsula, the morphological behaviour is dominated by the dynamics of the lagoon entrance. Soon after construction of the peninsula, a spit developed, squeezing the lagoon entrance. In the first months, the spit mostly elongated along the adjacent coast and widened to about 300–400 m (②). The crest level of the spit is approximately similar to the high water level (NAP +1.2 m), such that it is flooded during high tide and storms. The tidal channel into the lagoon migrated to the northeast and extended considerably over time (③). Strong velocities of over 1 m/s were observed here during rising and falling tide. The accretion on the southern side of the ZM is attributed to the local reduction in net sediment transport capacity (④). Changes on the dry beach were small; i.e. order of 0.2–0.3 m lowering after one year.

The observed cumulative volume changes during the study period (August 2011–August 2012) and concurrent wave heights and surge levels are shown in Fig. 4. To facilitate a detailed analysis, the study area has been divided into three control sections as illustrated in Fig. 2b: Peninsula (i.e. the main central part of the ZM), and Northern and Southern sections (i.e. adjacent coast to the northeast and southwest of the ZM). The control areas cover the area from approximately NAP −10 m to NAP +3 m. By August 2012, approximately 1.7 million m^3 had eroded from the peninsula area while about 1.2 million m^3 had accreted along the adjacent coastal sections (see Fig. 4a). Consequently, it appears that about 0.5 million m^3 has been transported out of the overall survey domain; this volume may be constituted of cross-shore (both offshore and landward, into the dunes) and/or alongshore losses.

3. Modelling the initial morphological response of the Sand Engine and the adjacent coast

3.1. Model description

To understand the physical process governing the initial response of the ZM and the adjacent coast, first a morphodynamic model that can accurately reproduce the observed morphological changes in the study area (under concurrent forcing) needs to be established. To achieve this goal, the process-based numerical model Delft3D [17] is used here to compute hydrodynamics, waves, sediment transport and morphology under influence of tidal, wind, and wave-driven currents. The basic model structure (see Fig. 5) and Delft3D are fully described in Lesser et al. [17] and is therefore not further described here.

The target of the modelling exercise is to obtain a model hindcast (August 2011–August 2012) that accurately reproduces (1) the magnitude of volume changes and (2) the observed erosion and sedimentation patterns in the entire study area. It is envisaged that the model can then also compute the individual impacts of separate wave conditions, which is relevant for further analysis in this research. While Delft3D includes an option to employ a morphological acceleration factor to speed up morphodynamic simulations [24,22], no such acceleration was implemented here as model accuracy is of paramount importance in this application.

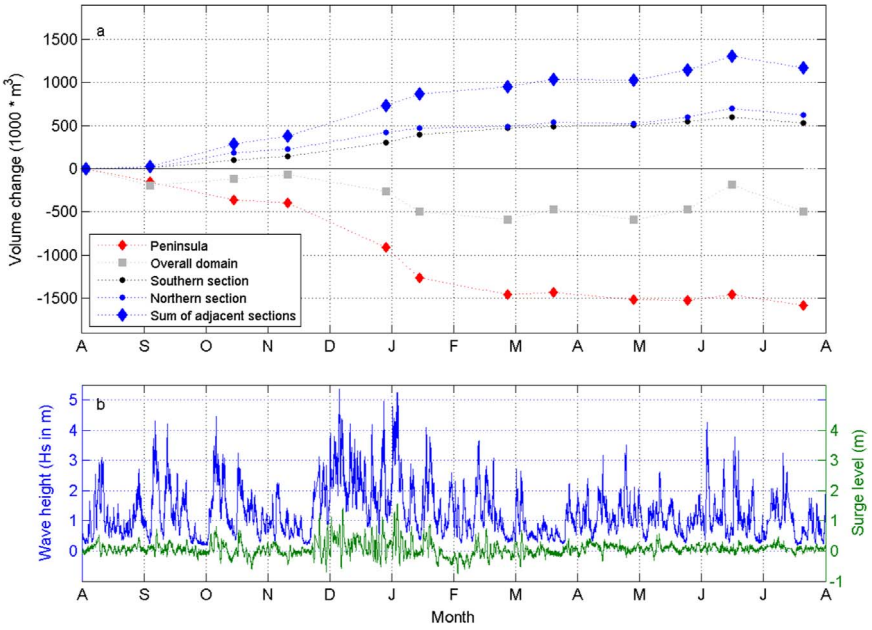

Fig. 4. (a) Cumulative volume change in the three different control sections (see Fig. 2b) from August 2011 till August 2012 (in million m^3; negative values indicate erosion) and (b) time series of the observed concurrent significant wave heights at Europlatform and observed surge levels at Hoek van Holland.

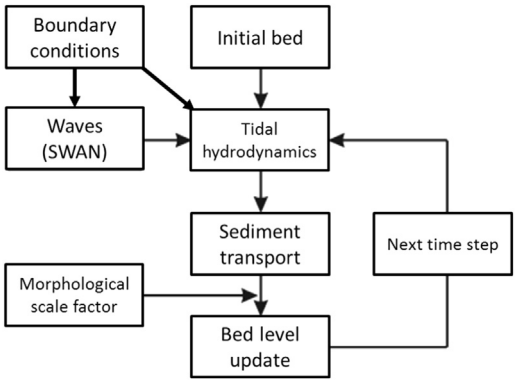

Fig. 5. Overview of the morphodynamic feedback loop applied in Delft3D.

3.2. Model implementation

The domain around the ZM was schematized with a curvilinear computational grid (indicated by the red box in Fig. 6b). The grid covers an area of 9.5 km in longshore direction and 4 km in cross-shore direction. The water depth at the offshore boundary is approximately 15 m. The grid resolution varies from 35 m to 135 m and the grid consists of 154 by 130 cells. The cell size increases with distance from the ZM. The bathymetry and the subaerial topography used in the model are based on the first survey conducted after completion of the ZM on 3 August 2011. Echo-sounding surveys conducted by Rijkswaterstaat in the last two decades are used for the remainder of the model domain (required for far-field tidal and wave models; see below).

The tidal boundary conditions for the model domain were retrieved via a series of nested hydrodynamic models to accurately incorporate the tidal characteristics along the Delfland coast and the generation of horizontal tidal currents. The simulations were conducted in depth-averaged (2DH) and hydrostatic mode. The large-scale Dutch Continental Shelf Model [44,29] was simulated for three months to provide tidal boundary conditions for the medium-scale Coastal Strip (*kustfijn*) model (see Fig. 6a) which, in turn, provided tidal information for the detailed Delft3D model covering the ZM. The tidal information was converted into astronomical components for the offshore boundary, while zero-gradient alongshore water level conditions (following the method described in Roelvink and Walstra [26]) were invoked on the lateral boundaries. Observed surge levels at Hoek van Holland (Fig. 4b) were added to the tidal water level forcing. Wind effects on the hydrodynamics were included by applying the measured 10-minute averaged wind time series from Hoek van Holland. All presented simulations were conducted in depth-averaged (2DH) and hydrostatic mode.

For the wave propagation modelling, three nested computational grids were applied. The large-scale wave grid with lowest resolution (Fig. 6b) was forced with measured time series of wave heights, periods and directions of the two offshore platforms Europlatform (EUR; see Fig. 2c) and IJmuiden Munitiestortplaats (IJM MSP). A uniform wind was applied based on the measured time series of wind conditions at Lichteiland Goeree (LEG). The large-scale wave grid which extends up to the location of the offshore wave buoys covers an area of about 79 km in longshore direction and 42 km in cross-shore direction, with varying grid resolution from about 170 m to more than 2000 m. The medium-scale wave domain (25 km by 13 km) was nested in the large-scale wave grid while the ZM wave domain (10.5 km by 4.5 km) was nested in the medium-scale domain. This degree of nesting, while computationally expensive, was required to ensure that the effect of refraction on the irregular bathymetry just north of the Port of Rotterdam was accurately represented in the ZM computations. The ZM wave domain is similar to the hydrodynamic model but has been extended by ~500 m in southern, western and northern direction.

Although the offshore wave observations shows large angles of incidence, the angle of incidence of the waves refracted towards the seaward edge of the surf zone (5 m) is not larger than 45° to shore-normal for significant wave heights up to 1.5 m; higher waves refract even more.

3.3. Model verification

All standard hydrodynamic parameters in Delft3D were kept at default settings for the 1-year long verification simulation. Modelled water levels, velocities and wave height were subjected to quantitative comparisons with field observations. The comparison statistics obtained are summarized in Table 2.

3.3.1. Water levels and currents

As the domain of the ZM model does not cover a permanent water level station, the water level verification was conducted with the kustfijn model for the station of Scheveningen. Besides a time series comparison between computed and observed water levels including wind and pressure effects (statistics are presented in Table 2), a period

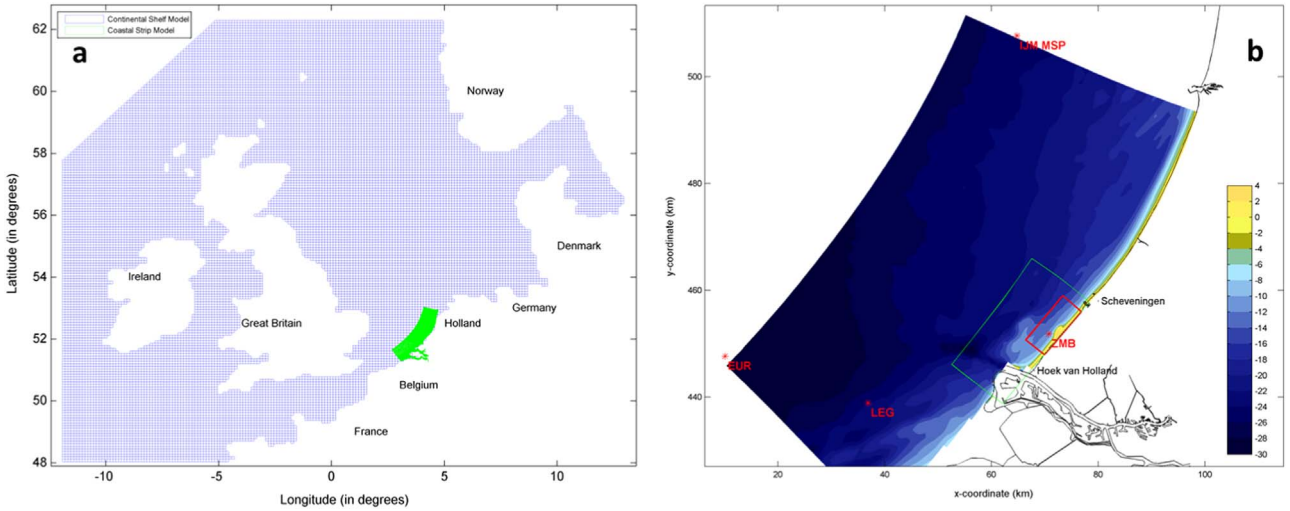

Fig. 6. (a) Cascade of hydrodynamic models: Continental Shelf Model (in blue) and Coastal Strip (kustfijn) model domains in green and (b) overall wave model domain and outlines of medium-scale (in green) and ZM wave model domains (in red; bed elevations in meters w.r.t. NAP). Note that the hydrodynamic model is equal to the ZM wave model, but slightly smaller. (For interpretation of the references to colour in this figure caption, the reader is referred to the web version of this paper.)

Table 2
Model verifications and comparison statistics.

Goal variable	Observation period of verification			Signal	Statistics		
	Start date	End date	Length		Corr.	R^2	RMSE
Water levels	1-Jun-2012	1-Aug-2012	61 d	Time series	0.98	0.95	0.14
				Tidal amplitude	Amplitude differences; see Table 3		
				Tidal phases	Phase differences; see Table 3		
Flow velocity	1-Jul-2012	4-Aug-2012	34 d	Current amplitude	Amplitude differences; see Table 3		
				Current phases	Phase differences; see Table 3		
Wave height	17-Dec-2011	25-Jan-2012	39 d	Time series	0.94	0.82	0.40

of two months was used for a detailed tidal analysis using T-tide [21]. Such an analysis omits all non-tidal effects. Modelled and measured water levels were compared and the differences for the six dominant tidal constituents were marginal with deviations in amplitudes up to 0.02 m and less than 12 min in phase (see Table 3).

The model performance for depth-averaged currents was evaluated against observations from ADCP location F (see Fig. 2b) for a period of 34 days (see Fig. 7a). Time series of the computed currents show the typical characteristics of the observed current magnitudes, but regularly underestimate the peak flood velocities during neap tides and overestimate ebb currents. The good correspondence of the measured (0.29 m/s) and modelled (0.30 m/s) main tidal constituent (M2) suggests that the increase in velocity is likely due to non-tidal effects, which in this case is probably the fresh water plume from the Rhine River which would enhance (retard) the tidal flow during the flood (ebb) phase.

3.3.2. Waves

Wave measurement data were available since the deployment of a nearshore wave buoy in mid-December 2011. The modelled and measured wave heights at the location of the nearshore wave buoy (water depth of 10 m) are shown in Fig. 7b for the first six weeks after installation. As this period captures sufficient wave events (with wave heights H_s up to 5.5 m), it was judged that this period was sufficiently long to verify the wave model performance. The model provides a very good representation of the nearshore waves during storms (both wave heights and time of occurrence), although the peak of the storm on the 5th of January 2012 is slightly underestimated. Overall, the correlation coefficient is 0.94 and the R^2 is 0.82. Model/data differences are larger when wave heights are lower than ~1.5 m. From a morphological point of view these mild wave conditions are expected to be of less importance; this will be further discussed in Section 4.

3.3.3. Morphology

A brute-force (MORFAC=1) simulation forced with tides, winds, surge and waves was undertaken for the 12 month study period (August 2011–August 2012). Analysis of the first model results showed that significant bed level changes (of more than 0.1 m) only occurred for wave heights higher than 1.5 m. As the focus of this study is on erosional/accretional behaviour the bed level changes were used as a diagnostic to eliminate certain wave conditions from the computation. Wave conditions with a wave height below 1.5 m and those with waves directed away from the coast (between nautical angles 30 and 180), which resulted in a combined total of 55% of the year, were omitted from the simulation, resulting in a 40% reduction of the computational effort. Applying the morphological model with its default formulations and (user manual suggested) parameter settings results in a morphological evolution that is quite far from observed (see Fig. 8).

Applying more advanced model features improved the results significantly. The best model/data comparison (see Fig. 9) was achieved with the settings shown in Table 4. Three key model features were found to be crucial to achieve a good model/data comparison: dry cell erosion, sediment transport formulation, and the formulation for nearshore wave energy distribution (i.e. wave and roller energy), which are discussed below.

The transition zone from wet to dry area is a dynamic area from a hydrodynamic point of view with interplay between tidal water level variations, tidal currents, wave- and wind-driven currents, swash and sometimes long waves. In present-day morphodynamic area models these processes are not fully resolved, but parameterisations have been made to enable dry areas to erode. In Delft3D, this is facilitated via a dry cell erosion feature which distributes the erosion of the most landward wet cell amongst its the adjacent dry cells. In this way computational cells that were originally above the maximum water level (i.e. dry cells) can be gradually eroded and become active wet cells when the bed level is lower than the water level at a given moment. The distribution of the total amount of erosion over the two cells is predefined by the user with, for example, a setting of 1(0.5) transferring 100% (50%) of the erosion in the wet cell to the adjacent dry cell. Based on a number of sensitivity tests a dry cell erosion factor of 1 gave the best model/data comparison for the hindcast presented in this study.

Of the several sediment transport formulations available in Delft3D, the best comparison between modelled and measured morphological change was obtained with the Van Rijn [38] formulation. Especially, the Van Rijn [38] formulation performs best in the deposition area where more sand is deposited higher up in the cross-shore profile (between NAP −1 m and NAP +2 m) which is in agreement with the observations. This is relevant for reproducing the spit development in the first year.

Table 3
Results of the statistical tidal analyses of water levels and currents.

Constituents	Water levels at Scheveningen				Constituents	Currents at ADCP F			
	Amplitudes (m/s)		Phases (min)			Amplitudes (m/s)		Phases (min)	
	Obs.	Mod.	Obs.	Mod.		Obs.	Mod.	Obs.	Mod.
O1	0.10	0.11	176	177	MU2	0.03	0.03	119	140
K1	0.09	0.11	338	335	N2	0.04	0.04	325	349
M2	0.78	0.76	68	73	M2	0.29	0.30	40	32
S2	0.17	0.18	136	137	L2	0.05	0.06	113	97
M4	0.22	0.22	103	114	S2	0.08	0.03	115	51
MS4	0.10	0.11	168	174	M4	0.01	0.04	2	81

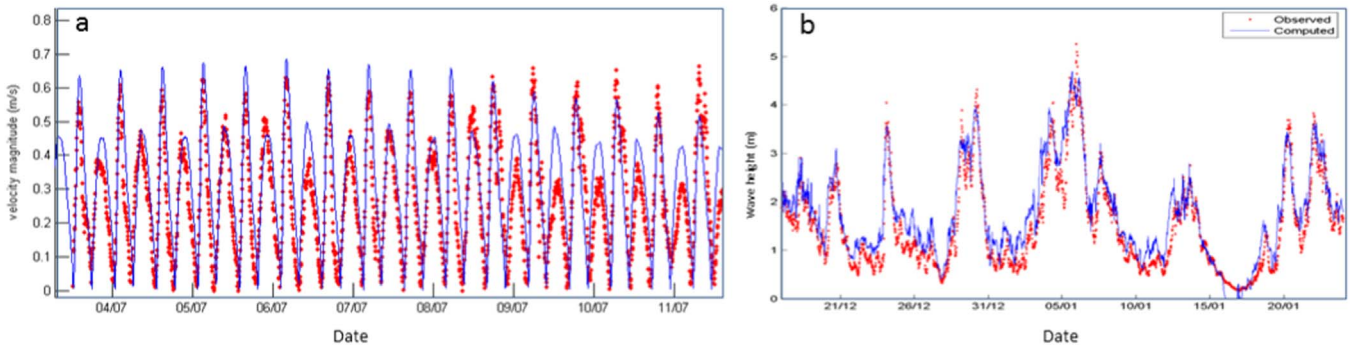

Fig. 7. (a) The comparison between computed and observed currents at location F for July 2012 (blue represents the computed currents) and (b) the computed and observed wave heights at the nearshore wave rider buoy for the period 17 December 2011 to 25 January 2012. See locations of the observations in Fig. 2b. (For interpretation of the references to colour in this figure caption, the reader is referred to the web version of this paper.)

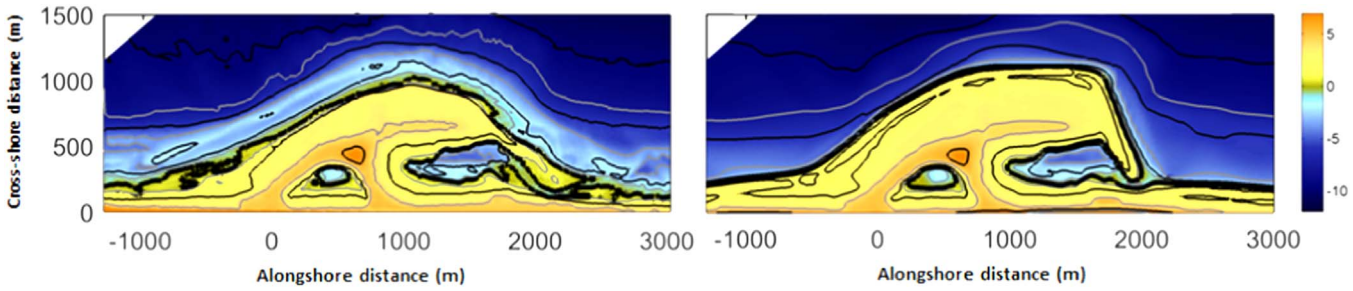

Fig. 8. (a) Observed bathymetry in August 2011; (b) model predicted bathymetry for August 2012 with default processes and parameter settings. The black depth contour lines represent the isobaths of −10 m, −6 m, −2 m, 0 m and +2 m. The 0 m contour is highlighted in both panels.

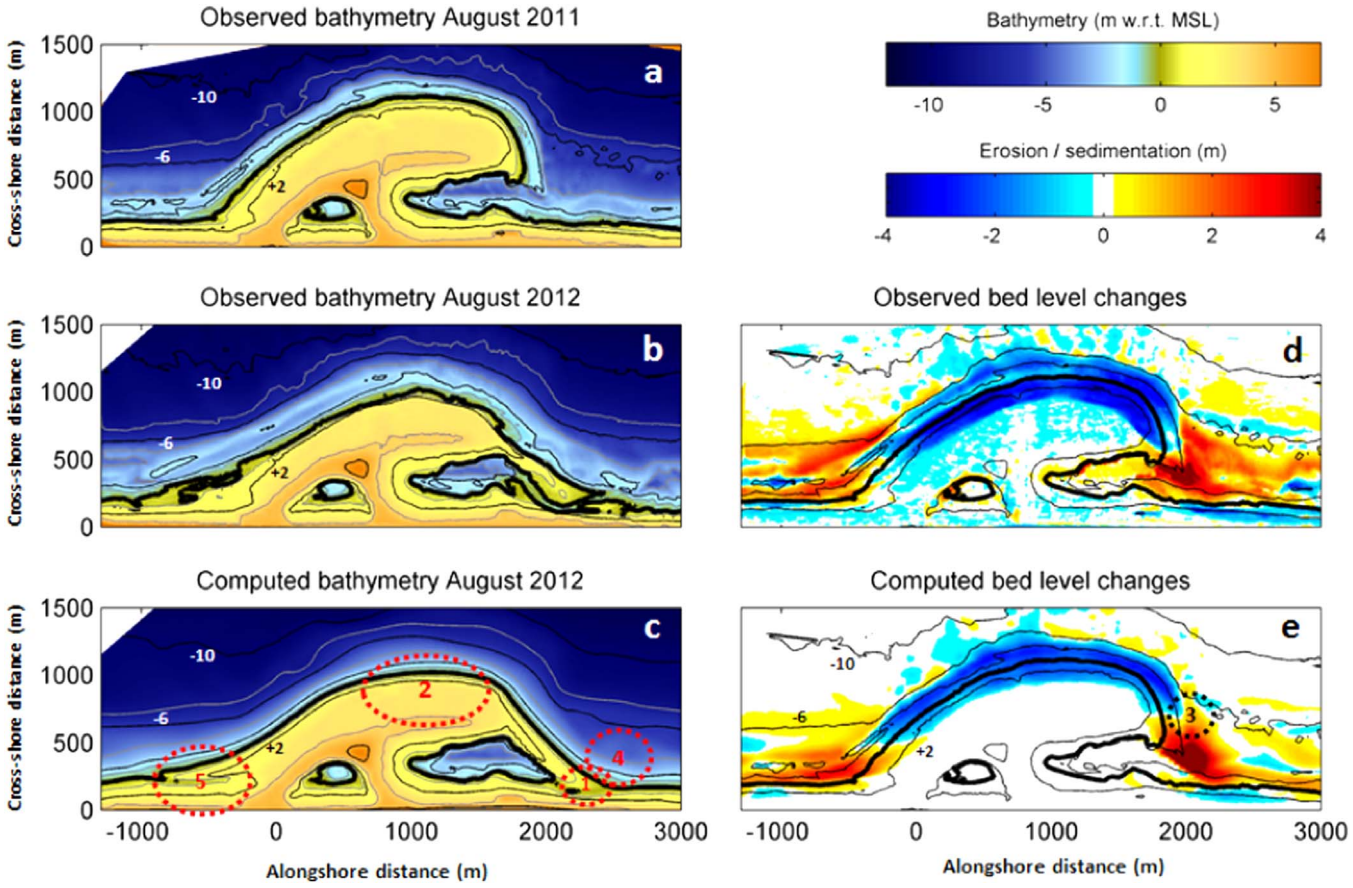

Fig. 9. (a) Observed bathymetry in August 2011; (b) observed bathymetry in August 2012; (c) model predicted bathymetry for August 2012; (d) and (e) observed and modelled bed level changes between August 2011 and August 2012, respectively. The black depth contour lines in (d) and (e) are based on the observed bathymetry of August 2011 for isobaths −10 m, −6 m, −2 m, 0 m and +2 m. The 0 m contour is highlighted in all panels.

Table 4
Model features and parameter settings applied in the Delft3D Sand Engine model.

Module	Parameter	Value	Description
Hydrodynamics	Roughness	Temporal and space-varying	Roughness predictor Van Rijn (2004)
	D_H	0.1 (m^2/s)	Horizontal eddy diffusivity
	V_H	1.0 (m^2/s)	Horizontal eddy viscosity (space-varying due to wave breaking)
Waves Roller model	γ	Variable	Wave breaking with variable gamma scheme (Ruessink et al. 2003)
	Gammax	0.7	Limiter to ensure wave breaking on time step level in Delft3D
Transport	D_{50}	300	Median grain size
	Formulation	Van Rijn (2004)	Sediment transport formulation
Morphology	*ThetSD*	1.0	Factor for erosion of adjacent dry cells
	MORFAC	1.0	Morphological acceleration factor

Two different nearshore wave models (the output of which is used by Delft3D-FLOW module to compute wave driven currents) that are dynamically linked with Delft3D-FLOW were tested: SWAN [2] and the so-called Roller model [23]. Of these two options, the Roller model was found to give the best model/data comparison. This is probably because only the Roller model incorporates the effect of breaker delay, parameterized by Roelvink et al. [25], due to the presence of the surface roller [9]. The surface roller is a phenomenon that occurs when waves break in the nearshore. When irregular waves break, (part of) the organised wave energy is converted into a surface roller. In a numerical modelling sense, the presence of the roller results in a non-zero fraction of broken waves [1] farther into the surf zone than without the roller. This, in essence, enhances onshore sediment transport and shifts the peak of the cross-shore distribution of the longshore current. In the roller formulations in Delft3D, the variable gamma scheme [27] results in a better agreement of the modelled and observed morphodynamics similar to the findings by Hsu [14].

Selecting and applying these more advanced options comes at a cost: these simulations are a factor 2 more computationally expensive than the default simulation, mainly due to the Van Rijn [38] transport formulation which has several iterative approximations built in. The simulation with the best model performance required a computational effort of 20 days on a Core i7-2600 CPU machine (at 3.40 GHz). The results of this simulation have been compared to the observed initial morphological evolution of the ZM and the adjacent coast both via visual comparison and an objective skill score test (Brier Skill score) discussed in the next sections.

3.3.4. Visual comparison

Modelled and measured bed level change over the 12 month study period generally compare rather well (see Fig. 9). The model correctly reproduces the development of a spit and a channel. The model predicted spit is however slightly less elongated compared to that observed while the channel is slightly shallower than the measurements indicate (see ① in Fig. 9c). The observed erosion of the most seaward part of the peninsula is generally well reproduced by the model (②). The observed shoreline retreat of about 100 m and the extent of the erosional area are accurately reproduced by the model. The most seaward depth contour above which significant erosion occurs (NAP −6 m) is very similar in the model and observations. The observed bar around NAP −3 m is smoothed out in the model which is unavoidable given the 2DH approach. The transition zone between erosion and sedimentation in the northern part of the ZM is generally well reproduced by the model (see ③ in Fig. 9e). The cross-shore dominated bar behaviour to the north of the ZM is not reproduced by the model, again due to the 2DH modelling approach adopted (see ④ in Fig. 9c). Sedimentation to the south of the ZM is also well reproduced by the model.

The modelled plan shape evolution of the ZM is sensitive to the method adopted to affect erosion of the dry areas and the applied sediment transport formulation. The updrift part (section south of the ZM) experiences large accretion due to the blockage of the longshore transports from the south. This results in the shoreline rotating to be perpendicular to the dominant south-westerly wave direction. The middle section (②) is also sensitive to the applied dry cell erosion method, also influencing the orientation of the downdrift part of the shape.

3.3.5. Brier Skill score

The Brier Skill Score (BSS) is commonly used as a measure of morphodynamic model predictions [39,34,28,22,3]. The BSS approach defined by [34] is adopted to evaluate the model skill:

$$BSS = 1 - \frac{MSE}{MSE_{ini}} \tag{1}$$

where MSE is the mean-squared error and MSE_{ini} the MSE of the reference prediction for which the initial bed is taken (zero change reference model). Therefore, the BSS can be interpreted as the model added skill relative to a prediction that nothing changes. A prediction that is as good as the zero change reference prediction receives a score of 0 and a perfect prediction a score of 1. A value between 0 and 1 can be interpreted as the proportion of improvement over the reference prediction. For a balanced appreciation of model performance [3] recommend that multiple accuracy and/or skill metrics are considered in concert; e.g. decomposition of the BSS would give relevant information on the phase, amplitude and bias. Given the focus of this paper, the analysis is restricted to the BSS in combination with the MSE and details on a decomposition analysis are not yet discussed.

The monthly modelled and measured bathymetries, within the survey domain (three control areas) between NAP −10 m and +3 m, were used to calculate the temporal evolution of model skill for the ZM model (see Fig. 10a). As the BSS does not reflect an absolute accuracy the mean-squared errors are presented in Fig. 10b. The BSS can be seen to increase in time, whereas the accuracy of the modelled bed levels decreases with time due to some deviations between modelled and observed bed elevations until it becomes more or less constant after February. Negative values of BSS are computed for the month of September and October (value of −2 and −0.03 resp.) as the bed changes in the first months are relatively small compared to the MSE, the latter partly being governed by interpolation errors of the initial bathymetry (Fig. 10b), leading to a negative value for BSS. In the following months, with higher wave energy and hence larger bed level changes, the BSS improves rapidly to 0.4 in January after which the score steadily increases to a value of 0.59 by August 2012 which is judged as 'Excellent' according to the classification proposed by Sutherland et al. [34].

After February, when the MSE becomes more or less constant, the increase of the BSS is governed by the MSE_{ini} which continues to increase as a result of the natural development away from the initial situation. The increase of the BSS over time may be explained as the emerging of longer, more skilful scales [3] and could illustrate that the processes governing the erosion of the ZM over time are well reflected by the model and have a larger relative contribution to the skill further in the simulation than in the first months.

In all, the model/data comparison demonstrates that the model can predict the redistribution well, such that the model can be used to examine the processes driving the morphological evolution.

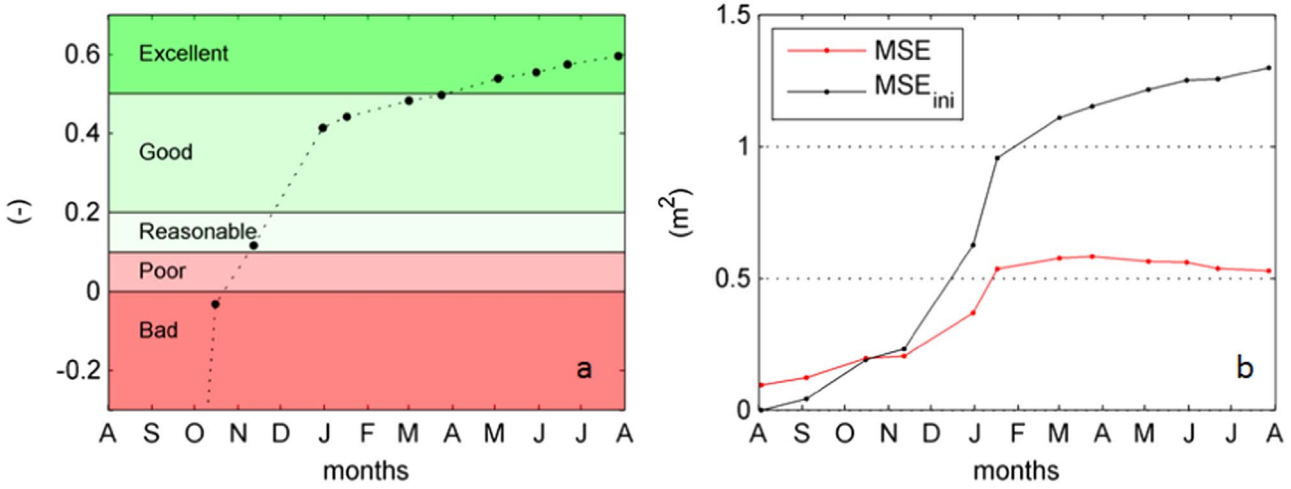

Fig. 10. (a) Model performance per month from August 2011 to August 2012; the colours represent the BSS classification following Sutherland et al. [34]; and (b) monthly mean square errors. (For interpretation of the references to colour in this figure caption, the reader is referred to the web version of this paper.)

3.4. Morphological verification 2012–2014

Following the successful model hindcast of the first year ZM evolution, a verification simulation was also conducted for the period August 2012 till August 2014; so, year 2 and 3 after completion of the ZM. The observed August 2012 bathymetry is used as initial model bathymetry of this verification simulation. The measured forcing conditions, such as waves, wind and surges, for this 2-year period were compiled and applied to the model in an exact same way as the first year (calibrated) run. Fig. 11 shows the bed levels and erosion/sedimentation pattern computed after two years. A BSS score of 0.43 was achieved, which is classified as a good comparison by Sutherland et al. [34]. This provides reasonable confidence in the predictive capability of the calibrated model.

Despite the good overall data/model comparison, computed shoreline positions show some deviations from the observations. This could be attributed to the lack of two processes in the present modelling: aeolian transports and sediment sorting. De Vries et al. [7] highlighted

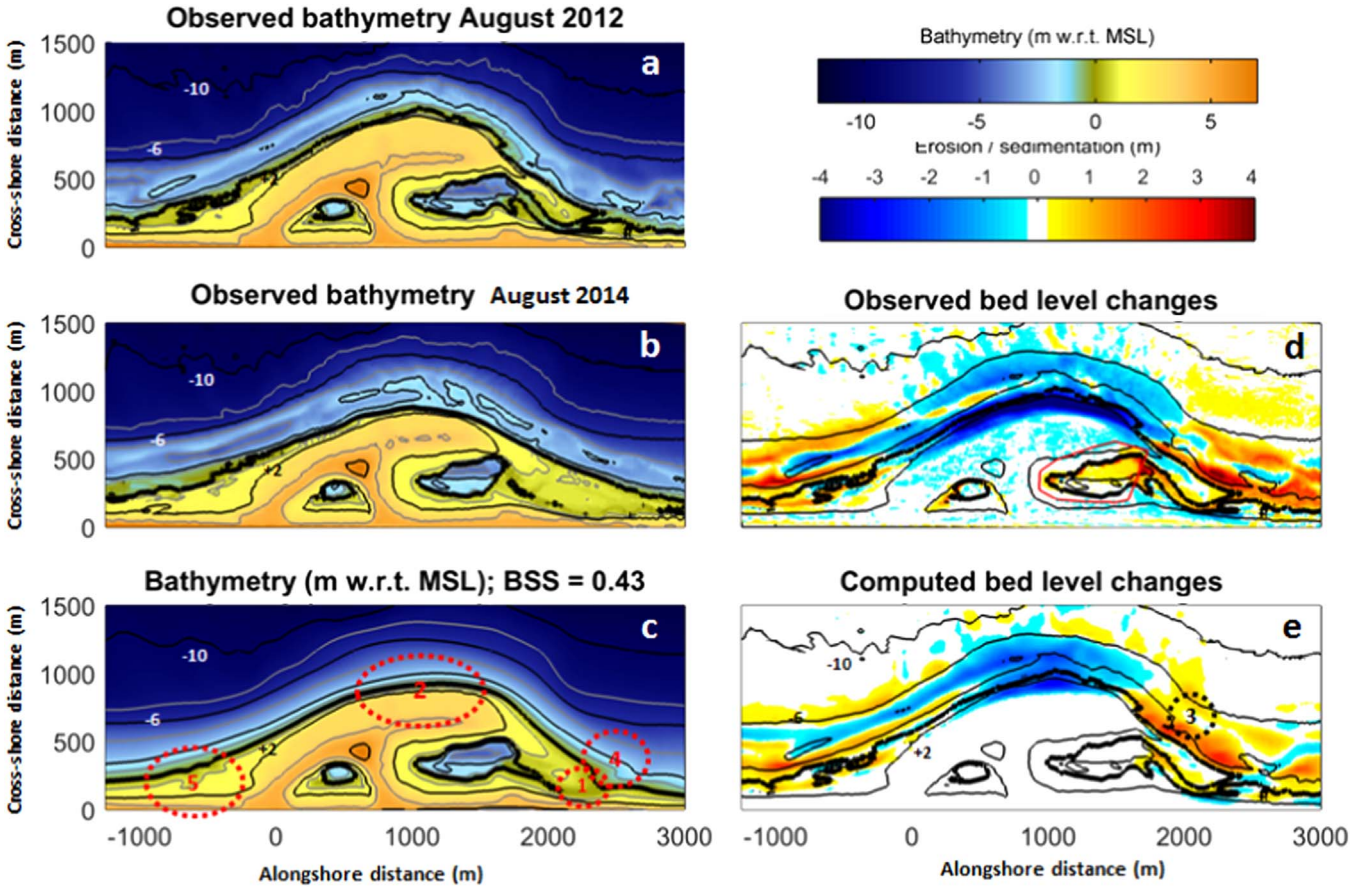

Fig. 11. (a) Observed bathymetry in August 2012; (b) observed bathymetry in August 2014; (c) model predicted bathymetry for August 2014; (d) and (e) observed and modelled bed level changes between August 2012 and August 2014, respectively. The black depth contour lines in (d) and (e) are based on the observed bathymetry of August 2012 for isobaths −10 m, −6 m, −2 m, 0 m and +2 m. The 0 m contour is highlighted in all panels.

the relation between the width of the wet intertidal area to the aeolian transports. Observations of sedimentation volumes in the dune lake and lagoon for year 2 and 3 indicate that the majority of this volume is transported from the intertidal area as the crest of the Sand Motor stabilized after the first year mainly due to armouring. Preliminary estimates indicate that the aeolian transports can be as high as 30 m^3/m/year or even more, which is in line with De Vries et al. [8]. Translating this transport into a bed level change would mean an absolute lowering of more than 0.5 m across the intertidal area assuming an averaged width of the intertidal area of 100 m. Observations have shown that the D_{50} at the most seaward part of the ZM is coarsening over time while some patches of finer sand have been found north and south of the ZM. In the present simulation the sand fraction is represented by only one D_{50} (and a standard D_{10}/D_{90} relation). Coarsening of the seaward part of the Peninsula will reduce its erodibility over time.

Future work will focus on the flexible incorporation of XBeach (nonstationary) in medium-term Delft3D morphological predictions coupled with a process-based aeolian transport model. The coupled model will be based on a flexible mesh to better resolve the surf zone dynamics and the corresponding transition between dry-wet areas on longer time scales using multiple sediment fractions. This approach will be used to examine the medium term (5–10 years) skill for large scale nourishments and the limits to process-based modelling of sandy interventions.

4. Governing processes

4.1. First year erosional behaviour

To enable a detailed investigation of physical processes that govern the observed morphological evolution during the study period, the ZM simulation results for the first year were analysed by extracting hourly bed levels and integrating the changes in the three control areas; viz. the Peninsula, the Northern adjacent section and the Southern adjacent section (see Fig. 2b). In general, the temporal evolution of the computed sediment volumes match well with the observed volume changes (see Fig. 12).

The model computes a total erosion volume on the Peninsula of about 1.24 million m^3 by August 2012, while the sum of the accretion volumes in the adjacent coastal sections is 1.22 million m^3. Thus about 20,000 m^3 of sand (~1.5% of the total eroded volume) appears to have moved out of the control areas, which is expected to have moved further alongshore or in cross-shore direction. The measured accretion volumes in both the northern and southern coastal sections are well reproduced by the model. Hence, the model results show that the redistribution of the ZM sand in the first year has largely been limited within the boundaries of the control areas. In contrast, the observations indicate that a net volume of about 450,000 m^3 was moved out of the control areas after the first year. This difference is likely due to landward movement of sand from the intertidal and subaerial beach to the dunes due to aeolian transport, which is included in the measurements but not simulated by the model. Possibly, although limited, a part of the deficit may be attributed to consolidation and redistribution in alongshore direction. Bathymetric surveys have shown a lowering of the bed level of about 0.2 - 0.3 m at the emerged part of the peninsula (above MSL) after the first storm months, which remains rather constant thereafter (see Fig. 9d). When neglecting the erosion of the (permanent) dry beach area of the ZM in the first year, the remaining observed loss is very comparable to the long-term natural background loss found at this coastal stretch of ~5 km; i.e. 300,000 m^3/year.

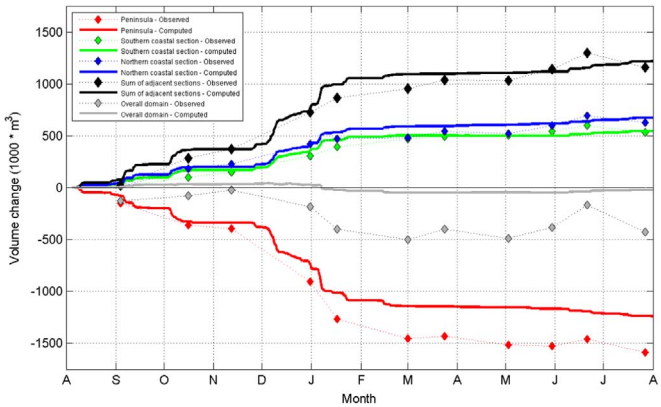

Fig. 12. Observed (symbols) and computed (solid lines) volume changes for the ZM peninsula and two adjacent coastal sections (north and south). Note that the red diamonds represent the area up to NAP +3 m. (For interpretation of the references to colour in this figure caption, the reader is referred to the web version of this paper.)

The spatial distribution of the cumulative sediment transport volumes over the 12 month study period (see Fig. 13) shows a northward net transport of about 170,000 m^3 along the undisturbed coast (at x=−1500 m) which is in general agreement with the reported annual net sediment transport rate for the Delfland coast [36]. Upon encountering the ZM (from the southern end, or the left hand side of Fig. 13), the longshore transports immediately (at about x=−750 m) reverse direction to the south. Further along the ZM, the longshore transport gradually increases to a peak southward transport of 160,000 m^3 at about x=−600 m and then decreases and changes direction back to northward around x=200 m. The northward transport reaches values of about 450,000 m^3 near the tip of the ZM (at x=1400 m), where the shoreline orientation is similar to the undisturbed coast. At this location, the higher transport rate compared to the undisturbed shoreline is likely due to the steeper profile of the seaward slopes of the ZM [16,19,5]. Just north of the tip (at x=2200 m), the transports increase up to approx. 550,000 m^3. Further north the northerly transport decreases to a minimum of 150,000 m^3 (x=3000 m) and thereafter increases again to the ambient longshore transport rate of 170,000 m^3/year.

Sediment from the peninsula is transported to the south at a rate of 160,000 m^3/year (at x=−600 m) while a volume of 550,000 m^3 is transported per year to the north (at x=2000 m), resulting in a sediment loss of approximately 710,000 m^3 from the peninsula. Converting the sediment transports (excluding pore volumes) to volume changes, assuming a porosity of 40%, leads to a calculated eroded volume of 1.18 million m^3 which is comparable to the 1.24 million m^3 presented in Fig. 12.

To illustrate the spatio-temporal bed level changes in the study area, the cross-shore integrated daily volume changes are presented as a time-stack in Fig. 14. The figure presents the daily volume changes integrated over each cross-shore transect along the ZM. The central area of the ZM is subject to almost continuous erosion during the first year, intensified during the higher wave events. In summer, lower waves from the NW cause slight sedimentation in this area. It is evident that the spit development starts at approx. x=1700 m; sedimentation (red colours) is indicated almost from day 1. Just downdrift of the spit, consistent erosion takes place followed by a less pronounced second band of sedimentation. The sedimentation pattern in the south (around x=−800 m) is more stable. The results show that during the largest wave events, the ZM impacts the bed levels over a relatively large area of about 6 km alongshore (from x=~−2000 m to x=~4000 m).

4.2. Erosion due to wave events

Both Figs. 12 and 14 indicate that the most dominant morphodynamic process occurring at the study site is erosion of the ZM during high energy wave events and the deposition of the eroded sand along the adjacent coast (both to the north and south of the ZM). Therefore, to investigate the dependencies between the morphological behaviour

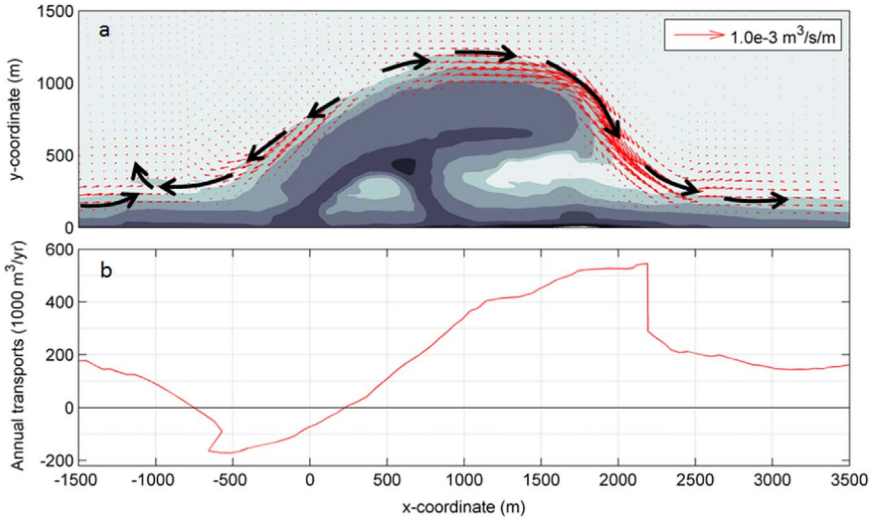

Fig. 13. (a) Computed yearly averaged sediment transports (represented by the red arrows), while the thick black arrows (drawn to a qualitative scale only) indicate the main cumulative transport pathways over the study period, and (b) yearly-averaged longshore transport curve along the ZM. (For interpretation of the references to color in this figure caption, the reader is referred to the web version of this paper.)

and environmental forcing conditions, high energy wave events were determined on the basis of the integrated wave energy over individual events (i.e. meteorologically independent events). Here, a high energy wave event is defined as a consecutive period (duration) over which the offshore significant wave height is higher than 2 m. The 12 largest high energy wave events during the study period thus determined were extracted for further analysis. Assuming a Rayleigh distribution of waves, the integrated wave energy density ∑ E was determined for each event as follows [31]:

$$\sum E = \int_0^N \frac{1}{16}\rho g H_s^2 \Delta t \tag{2}$$

where ρ is the density of sea water (kg/m^3), g is gravitational acceleration (m/s^2), H_s is the significant wave height (m), ∆ is the time interval of measurements (s), and N is the total duration of the storm. The integrated volume changes of the peninsula for the 12 events with the highest wave energy density are presented in Fig. 15. For reference, the events are chronologically numbered (see Fig. 15c). The largest total net sediment loss (185,000 m^3) from the peninsula occurs during storm event #9 (2nd of January 2012, southwesterly waves, mean H_s of 3.7 m, duration approx. 90 hours).

Fig. 15b shows the averaged and maximum wave height for each considered wave event. Generally, with increasing wave heights more erosion is computed, but there is too much variation to define a strong relation. The duration of a storm event shows an increasing relation with eroded volume for events with durations exceeding 72 hours (see Fig. 15a). Analysis of the 12 different storm events shows that the computed erosion volume for a given storm is proportional to the integrated wave energy density of an individual storm (see Fig. 15c). Wave directions during the considered wave events do not seem to play an important role as the e.g. six largest storms are close to a linear

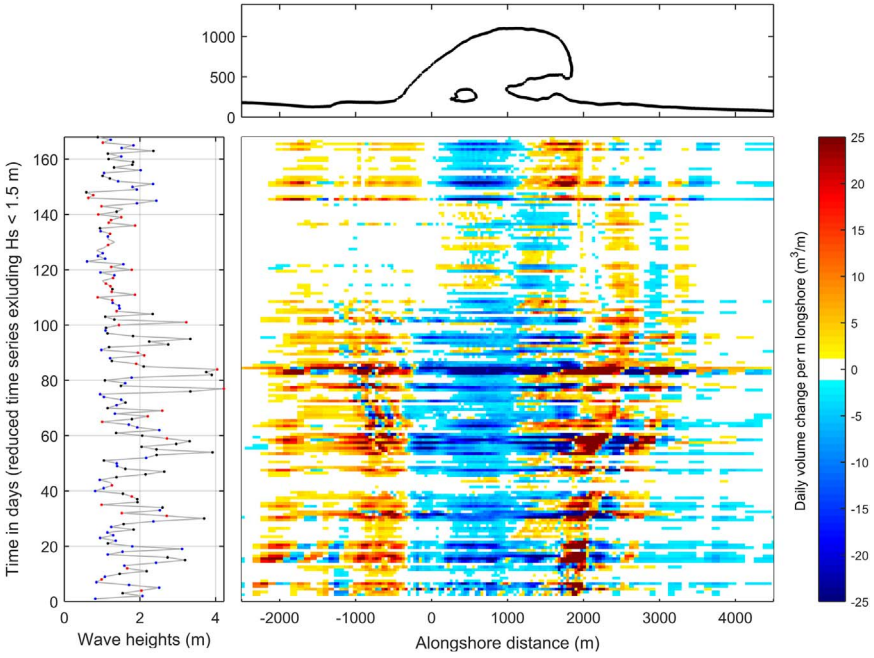

Fig. 14. Time-stack of daily volume changes integrated per cross-shore transect (from NAP −5 m to NAP +2 m). Blue patches indicate erosion; yellow / red indicate sedimentation. The left panel shows concurrent daily-averaged wave heights. Black/red/blue dots represent south-westerly/north-westerly/westerly waves. (For interpretation of the references to colour in this figure caption, the reader is referred to the web version of this paper.)

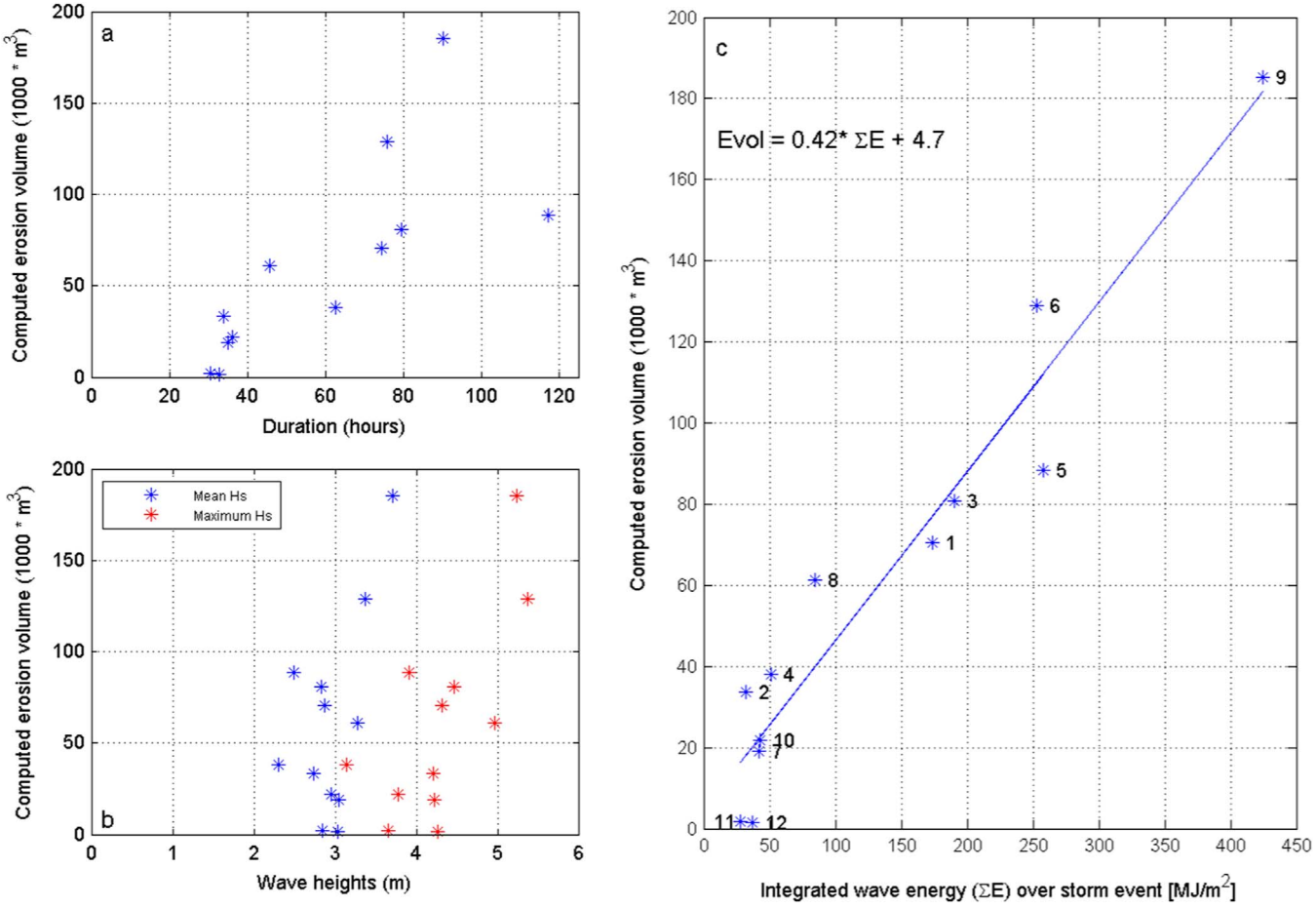

Fig. 15. Computed ZM erosion volume for the 12 identified high energy wave events versus (a) the storm duration, (b) the averaged and maximum wave height per event and (c) the integrated wave energy during the event. The numbers in (c) indicate the sequence of the event during the year.

dependency while these storms had different predominant wave directions (see Fig. 15c). Model results indicate that due to the shape of the ZM waves higher than about 2 m cause a divergence point in the wave-driven currents, whereby the angle of the incoming waves determines the location of the divergence point. In the divergence zone erosion will occur due to the opposite sediment transports directions. So the wave direction does influence where along the ZM most erosion takes place during a given wave event. But the erosion volumes in Fig. 15 are aggregated over the entire ZM which is why they are more correlated with wave height than with wave direction.

Although, individual events with high wave energy densities result in large erosion volumes, the sum of the erosion volumes of the 12 largest events account only for about 60% of the measured erosion volume on the Peninsula [18]. The stormy months of December 2011 and January 2012 are responsible for approximately 60% of the total erosion volume. Events with high wave energy densities accelerate the erosion of the peninsula, while a gentle trend of erosion is observed during the rest of the year when milder conditions occur.

4.3. Relative contributions of environmental forcings

To gain insights into the relative contributions of the various environmental forcings to the initial morphological response of the ZM, a series of simulations where the different forcing processes were sequentially eliminated was undertaken using the verified model. The forcing types thus investigated were: horizontal and vertical tide, storm surge, wind and waves. This investigation comprised six separate simulations (see Table 5), wherein the reference case (Run A) is the above described brute-force simulation with all available processes activated.

Table 5
Overview of simulations with different types of forcing.

Simulation	Forcing types applied
Run A: Reference run	Wave effects, vertical tide, wind-driven currents, surge levels, horizontal tide
Run B	Wave effects, vertical tide, wind-driven currents, surge levels
Run C	Wave effects, vertical tide, wind-driven currents
Run D	Wave effects, vertical tide
Run E	Wave effects only
Run F	Run E, but without wave effects

The evolution of the computed erosion volume of the ZM Peninsula through the study period is shown for each simulation in Fig. 16. Note that several sets of simulations were undertaken to assess whether the order of elimination of the different forcing (except for the wave forcing, which was always present) would affect the results. All such sets of simulations showed similar results and therefore only one selected set is discussed below.

Neglecting the horizontal tide from the reference run has a very limited effect on the erosional behaviour; a difference of only 3% in the total reference erosion volume. Similarly, eliminating the surge levels and wind-driven currents has minor effects; both contribute less than 5% of the total erosion volume. However, the vertical tidal variations result in a significant contribution of 17% of the cumulative erosion volume. The vertical tide is expected to influence the active part of the cross-shore profile and as such affect the erosion volumes (i.e. a larger part of the coastal profile will be mobilized when water levels vary over

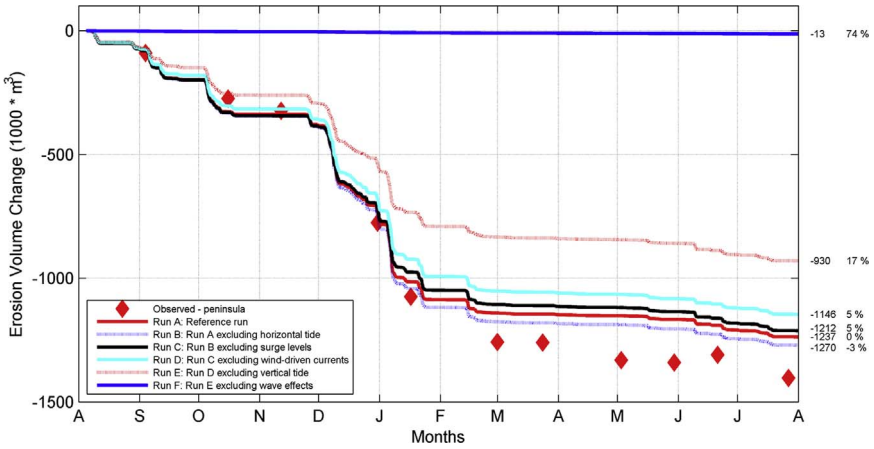

Fig. 16. Volume changes of the ZM over the study period showing the relative contribution of the different environmental forcings. The columns on the right give the final computed volume change per simulation and the difference with respect to the reference run in terms of percentage.

time). The model predictions indicate that waves are by far the dominant forcing mechanism. Wave effects, leading to wave-driven currents and enhanced bed shear stresses, contribute to approximately 75% of the total erosion volume.

The above is in line with the findings from Grunnet et al. [12]. After investigating the relative contribution of forcings on a shoreface nourishment at a barrier island, Grunnet et al. [12] concluded that the horizontal tide had a negligible effect on the transports, but that the vertical tide played a significant role. Results presented above support the suggestion of Grunnet et al. [12] that a more simplified approach where the horizontal tide is omitted may be justifiable in some situations. Such an omission would save significant efforts in deriving the tidal currents and schematising it for longer-term predictions, increasing the potential of process-based modelling for the design and evaluation of coastal engineering projects.

5. Conclusions

The anticipated increase in global nourishment volumes and size and the request for more complex nourishment shapes demands adequate predictions of the morphodynamic evolution of such sandy interventions. Yet, the skill of current state-of-the-art models for such projects are not known as well as the primary drivers that control this behaviour. A process-based model has been used to successfully hindcast the initial response of the Sand Engine mega-nourishment in The Netherlands. The Delft3D model reproduces measured water levels, velocities and nearshore waves well. Applying the morphological model with its default formulations and parameter settings results in a morphological evolution that is quite far from observed. Three key model features were found to be crucial to achieve a good model/data comparison: the erosion of dry cells, sediment transport formulation, and the formulation for nearshore wave energy distribution. Applying these features results in a computed morphological evolution which is consistent with the measured evolution during the study period, with Brier Skill Scores in the 'Excellent' range following the classification of Sutherland et al. [34]. Model results clearly showed that the sand eroded from the main peninsular section of the Sand Engine is deposited along adjacent north and south coastlines, accreting up to 6 km of coastline in total during just the first year of the Sand Engine.

Analysis of the model results indicated that the erosional behaviour of the Sand Engine has a linear dependency on the cumulative wave energy of individual high energy wave events, with the duration of a storm event being more dominant than the maximum wave height occurring during the storm. The wave directions during the events appear to be irrelevant for the erosional behaviour of the nourishment. The integrated erosion volume due to the 12 events with the highest cumulative wave energy events sums up to approximately 60% of the total eroded volume at the peninsula after one year. The less energetic storm events, with a higher probability of occurrence, are hence equally important for the initial response of the Sand Engine.

Further analysis of the relative contributions of the different environmental forcings to the total erosional behaviour of the nourishment using the verified model indicated that wave forcing dominated the initial morphological response of the Sand Engine, accounting for approximately 75% of the total erosion volume after the first year. The vertical tide is the second most contributing factor accounting for nearly 17% of the total erosion volume, with horizontal tide, surge and wind playing only a very minor role (all accounting for less than 5% of the total erosion volume).

Acknowledgements

This work is funded by NatureCoast, a project of technology foundation STW, applied science division of NWO. Roshanka Ranasinghe is supported by the AXA Research Fund and the Deltares Harbour, Coastal and Offshore Research Program Coastal Developments. Bas Huisman and Marcel Stive are partially supported by the ERC-Advanced Grant 291206 - NEMO. Field data was collected by the Dutch Ministry of Infrastructure and the Environment (Rijkswaterstaat) with the support of the Province of South-Holland, the European Fund for Regional Development EFRO and EcoShape Building with Nature. The constructive comments of the anonymous reviewers are much appreciated and helped to improve the manuscript.

References

[1] J.A. Battjes, J.P.F.M. Janssen, Energy loss and set-up due to breaking of random waves, in: 16th International Conference on Coastal Engineering, vol. 1, 1978, Hamburg, Germany. ASCE, pp. 570–587.
[2] N. Booij, R.C. Ris, L.H. Holthuijsen, A third-generation wave model for coastal regions 1. Model description and validation, J. Geophys. Res. 104 (C4) (1999) 17.
[3] J. Bosboom, A.J.H.M. Reniers, A.P. Luijendijk, On the perception of morphodynamic model skill, Coast. Eng. (2014) 94.
[4] J.G. de Ronde, J.P.M. Mulder, R. Spanhoff, Morphological developments and coastal zone management in The Netherlands, International Conference on Estuaries and Coasts, 2003.
[5] M.A. de Schipper, S. de Vries, B.G. Ruessink, R.C. de Zeeuw, J. Rutten, C. van Gelder-Maas, M.J.F. Stive, Initial spreading of a mega feeder nourishment: observations of the sand engine pilot project, Coast. Eng. (2016) 111.
[6] B. De Sonneville, A. Van der Spek, Sediment- and morphodynamics of shoreface nourishments along the north-holland coast, Coast. Eng. Proc. (2012).
[7] S. De Vries, S.M. Arens, M.A. de Schipper, R. Ranasinghe, Aeolian sediment transport on a beach with a varying sediment supply, Aeolian Res. (2014) 15.
[8] S. De Vries, H.N. Southgate, W. Kanning, R. Ranasinghe, Dune behavior and aeolian transport on decadal timescales, Coast. Eng. 67 (2012) 41–53.
[9] R.G. Dean, R.A. Dalrymple, Water Wave Mechanics for Engineers and Scientists, World Scientific Press, Singapore, 1991.
[10] E.P.L. Elias, A.J.F. van der Spek, Z.B. Wang, J.G. de Ronde, Morphodynamic development and sediment budget of the Dutch Wadden sea over the last century,

Netherlands J. Geosci. 91 (2012).
[11] N.A. Elko, P. Wang, Immediate profile and planform evolution of a beach nourishment project with hurricane influences, Coastal Eng. (2007) 54.
[12] N.M. Grunnet, D.J.R. Walstra, B.G. Ruessink, Process-based modelling of a shoreface nourishment, Coast. Eng. 51 (7) (2004) 581–607.
[13] A. Hendriks, The impact of re-surfacing groins on hydrodynamics and sediment transport at the delfland coast, Master's thesis, Civil Engineering, TU Delft, 2011.
[14] Hsu, Evaluation of delft3d performance in nearshore flows, Technical report, Ocean dynamics and prediction branch Oceanography Division. Naval Research Laboratory, 2006.
[15] B.J.A. Huisman, E.E. Sirks, L. Van der Valk, D.J.R. Walstra, Time and spatial variability of sediment gradings in the surfzone of a large scale nourishment, J. Coast. Res. 70 (2014) 127–132 [Special Issue No.].
[16] J.W. Kamphuis, Alongshore sediment transport rate, J. Waterways, Port, Coast. Ocean Eng., ASCE 117 (6) (1991) 624–641.
[17] G.R. Lesser, J.A. Roelvink, J.A.T.M. van Kester, G.S. Stelling, Development and validation of a three-dimensional morphological model, Coast. Eng. 51 (8-9) (2004) 883–915.
[18] A.P. Luijendijk, B. Huisman, M. In: De Schipper, Impact of a Storm on Proceedings of the First Year Evolution of the Sand Engine, in: Coastal Sediments 2015 Conference, 2015.
[19] J. Mil-Homens, R. Ranasinghe, J.S.M. van Thiel de Vries, M.J.F. Stive, Re-evaluation and improvement of three commonly used bulk longshore sediment transport formulas, Coast. Eng. (2013).
[20] J.P.M. Mulder, P.K. Tonnon, sand engine: Background and design of a mega-nourishment pilot in The Netherlands, Proceedings of the International Conference on Coastal Engineering, 2010, p. 32.
[21] R. Pawlowicz, B. Beardsley, S. Lentz, Classical tidal harmonic analysis including error estimates in matlab using t-tide, Comput. Geosci. (2002).
[22] R. Ranasinghe, C.M. Swinkels, A.P. Luijendijk, J.A. Roelvink, J. Bosboom, M.J.F. Stive, D.J.R. Walstra, Morphodynamic upscaling with the MORFAC approach: dependencies and sensitivities, Coast. Eng. (2011) 58.
[23] A.J.H.M. Reniers, J.A. Roelvink, E.B. Thornton, Morphodynamic modeling of an embayed beach under wave group forcing, J. Geophys. Res. 109 (C01030) (2004) 1–22.
[24] J.A. Roelvink, Coastal morphodynamic evolution techniques, Coast. Eng. 53 (2006) 277–287.
[25] J.A. Roelvink, T.J.G.P. Meijer, K. Houwman, R. Bakker, R. Spanhoff, Field validation and application of a coastal profile model, in: Proceedings Coastal Dynamics95 Conference, 1995.
[26] J.A. Roelvink, D.J.R. Walstra, Keeping it simple by using complex models, in: The 6th International Conference on Hydroscience and Engineering (ICHE-2004), Brisbane, Australia, 2004.
[27] B.G. Ruessink, D.J.R. Walstra, H.N. Southgate, Calibration and verification of a parametric wave model on barred beaches, Coast. Eng. 48 (3) (2003) 139–149.
[28] P. Ruggiero, D.J.R. Walstra, G. Gelfenbaum, M. van Ormondt, Seasonal-scale nearshore morphological evolution: field observations and numerical modeling, Coast. Eng. 56 (11-12) (2009) 1153–1172.
[29] D.C. Slobbe, M. Verlaan, R. Klees, H. Gerritsen, Obtaining instantaneous water levels relative to a geoid with a 2d storm surge model, Continental Shelf Res. (2013) 52.
[30] H.N. Southgate, Data-based yearly forecasting of beach volumes along the Dutch North Sea Coast, Coast. Eng. (2011) 58.
[31] K.D. Splinter, J.T. Carley, A. Golshani, R. Tomlinson, A relationship to describe the cumulative impact of storm clusters on beach erosion, Coast. Eng. (2014) 83.
[32] M.J.F. Stive, M.A. De Schipper, A.P. Luijendijk, S.G.J. Aarninkhof, C. Van Gelder-Maas, J.S.M. Van Thiel de Vries, S. De Vries, M. Henriquez, S. Marx, R. Ranasinghe, A new alternative to saving our beaches from sea-level rise: the sand engine, J. Coast. Res. 29 (5) (2013) 1001–1008.
[33] M.J.F. Stive, L.O. Fresco, P. Kabat, B.W.A.H. Parmet, C.P. Veerman, How the Dutch plan to stay dry over the next century, Proc. Inst. Civil Eng. Civil Eng. (2011) 164.
[34] J. Sutherland, A.H. Peet, R.L. Soulsby, Evaluating the performance of morphological models, Coast. Eng. 51 (8-9) (2004) 917–939.
[35] P. van de Rest, Morphodynamica an hydrodynamica van de Hollandse kust, Master's thesis, Delft University of Technology, 2004.
[36] L.C. Van Rijn, Sand budget and coastline changes of the central coast of holland between den helder and hoek van holland period 1964–2040; project kustgenese, 1995.
[37] L.C. Van Rijn, Sediment transport and budget of the central coastal zone of Holland, Coast. Eng. 32 (1997) 61–90.
[38] L.C. Van Rijn, Unified view of sediment transport by currents and waves. II: suspended transport, J. Hydraul. Eng. 133 (6) (2007) 668–689.
[39] L.C. van Rijn, D.J.R. Walstra, B. Grasmeijer, J. Sutherland, S. Pan, J.P. Sierra, The predictability of cross-shore bed evolution of sandy beaches at the time scale of storms and seasons using process-based Profile models, Coast. Eng. 47 (3) (2003) 295–327.
[40] P. Van Vessem, A. Stolk, Sand budget of the Dutch coast, Coast. Eng. Proc., 1990.
[41] K.M. Wijnberg, Environmental controls on decadal morphologic behaviour of the holland coast, Mar. Geol. (2002) 189.
[42] K.M. Wijnberg, J.H.J. Terwindt, Extracting decadal morphological behavior from high-resolution, long-term bathymetric surveys along the holland coast using eigenfunction analysis, Mar. Geol. 126 (1-4) (1995) 301–330.
[43] J. Wijsman, E. Verduin, T0 monitoring zandmotor Delftlandse kust: benthos ondiepe kustzone en natte strand, Imares Wageningen UR (2011).
[44] F. Zijl, M. Verlaan, H. Gerritsen, Improved water-level forecasting for the north-west European shelf and north sea through direct modelling of tide, surge and non-linear interaction, Ocean Dyn. (2013).